

**R&D OF A HIGH-PERFORMANCE DIRC DETECTOR FOR
USE IN AN ELECTRON-ION COLLIDER**

by

S. Lee Allison
MS in Physics

A Dissertation Submitted to the Faculty of
Old Dominion University in Partial Fulfillment of the
Requirements for the Degree of

DOCTOR OF PHILOSOPHY

PHYSICS

OLD DOMINION UNIVERSITY
May 2017

Approved by:

Dr. Charles Hyde (Director)

Dr. Grzegorz Kalicy (Member)

member (Member)

ABSTRACT

R&D OF A HIGH-PERFORMANCE DIRC DETECTOR FOR USE IN AN ELECTRON-ION COLLIDER

S. Lee Allison
Old Dominion University, 2016
Director: Dr. Dr. Charles Hyde

text of abstract goes here

Copyright, 2016, by S. Lee Allison, All Rights Reserved.

ACKNOWLEDGEMENTS

Contents

LIST OF TABLES	vii
LIST OF FIGURES	viii
Chapter	
1. INTRODUCTION	2
2. ELECTRON-ION COLLIDER	3
2.1 SCIENCE GOALS	4
2.2 FACILITIES	7
3. DIRC TECHNOLOGY	11
3.1 CHERENKOV RADIATION	11
3.2 APPLYING THE CHERENKOV EFFECT TO PARTICLE ID	12
3.3 RING IMAGING DETECTORS	13
3.4 DIRC DETECTORS	14
3.5 HIT PATTERNS AND CHERENKOV ANGLE RECONSTRUCTION METHODS	17
4. HIGH-PERFORMANCE DIRC@EIC	19
4.1 EVOLUTION OF THE DIRC@EIC DESIGN	19
4.2 CURRENT HIGH-PERFORMANCE DIRC DESIGN	19
4.3 SIMULATED PERFORMANCE	19
4.4 POTENTIAL OPTIMIZATIONS	19
5. TESTING DIRC COMPONENTS	20
5.1 OPTICAL PROPERTIES OF 3-LAYER LENS	20
5.2 RADIATION HARDNESS OF NLAK33 MATERIAL	21
5.3 PERFORMANCE OF MCP-PMTS IN HIGH MAGNETIC FIELD	21
6. 3-LAYER LENS PERFORMANCE IN PARTICLE BEAM	23
6.1 PROTOTYPE SETUP	23
6.2 SIMULATED PERFORMANCE	23
6.3 DATA ANALYSIS	23
7. OUTLOOK AND SUMMARY	24

BIBLIOGRAPHY	24
APPENDICES	
A. ERROR EVALUATION	27
VITA	28

List of Tables

List of Figures

2.1.	The reduced cross section $\sigma_r(x, Q^2)$ as a function of Q^2 . Filled circles are combined H1 and Zeus data from HERA for proton-positron collisions, hollow squares are from fixed target experiments, and the yellow is prediction from HERAPDF0.1	4
2.2.	Evolution of our understanding of nucleon spin structure. Left: In the 1980s, a nucleons spin was naively explained by the alignment of the spins of its constituent quarks. Right: In the current picture, valence quarks, sea quarks and gluons, and their possible orbital motion are expected to contribute to overall nucleon spin.	5
2.3.	Ratio of the nucleon structure functions for carbon and deuterium for $0.2 < x < 0.9$ and a range of Q^2 values.	6
2.4.	Momentum distributions for pions (blue) and kaons (magenta) from the pythia simulation package for DIS events corresponding to collisions between 10 GeV electrons and 100 GeV protons, a common BNL/JLab kinematic, shown for a bin of $10 < Q^2 < 100$ GeV 2	8
2.5.	Current design of the EIC facility for JLab with the two interaction points (IPs) highlighted in red (top), and the current baseline design for the detector at IP1 (bottom).	9
2.6.	Current design of the EIC facility at BNL (top), and the proposed BeAST (Brookhaven eA Solenoidal Tracker) detector (bottom).	10
3.1.	Illustration of the Cherenkov cone.	12
3.2.	Particle momentum [GeV/c] versus Cherenkov angle [mrad] for different particle species in fused silica ($n \approx 1.473$). The zoomed image shows that it is indeed possible to differentiate pions, kaons, and protons at higher particle momenta.	13
3.3.	Basic concept of a proximity focusing Ring Imaging Cherenkov (RICH) detector (a), and an example of how they can be used to do PID based on particle mass (b).	14
3.4.	The basic components of a DIRC detector: a solid radiator, typically fused silica (green); a mirror to redirect backward-going photons (pink); optional focusing optics (purple); an expansion volume to allow photons to separate in space (cyan); and a detector surface to record the position and arrival time of Cherenkov photons (maroon).	15
3.5.	Schematic of BaBar DIRC and imaging region.	16

3.6. Performance of the BaBar DIRC for $e^+e^- \rightarrow \mu^+\mu^-$ events. a) shows the difference between the measured and expected Cherenkov angle (dots) and a Gaussian fit to the data with a 2.5 mrad width (line). b) is the average number of detected photons vs. track polar angle for data (dots) and Geant4 simulation (line).	17
3.7. Evolution of the DIRC concept. From top left to bottom right: BaBar Barrel DIRC, Focusing DIRC, PANDA Barrel DIRC, PANDA Disc DIRC, Belle II Time of Propagation DIRC, LHCb TORCH DIRC, GlueX DIRC, EIC DIRC	18
5.1. Schematic drawing of the 3-layer lens design with two layers of fused silica sandwiching a layer of high refractive index NLaK33 glass (a), and a side and front view of a prototype lens built for testing (b).	20
5.2. Simulated hit pattern of PANDA DIRC without (black) and with (red) air gap lens focusing (a). On the outer edges of the ring image the lens is becoming dispersive and losing photons, while near the center of the rings the lens does a good job of focusing the image, as seen more clearly in b).	21
5.3. The simulated focal planes (red lines) of the 3-layer lens (left) and a 2-layer lens (right) compared to the shape of the expansion volume prism (grey). Obviously the focal plane of the 2-layer lens is highly parabolic in shape, whereas the 3-layer lens focal plane is relatively flat, allowing for a better resolution of the Cherenkov angle.	22

Comments

CHAPTER 1

INTRODUCTION

CHAPTER 2

ELECTRON-ION COLLIDER

It has been known for nearly a century that atoms are composed of nucleons (protons and neutrons), but it took another 50 years for Murray Gell-Mann and George Zweig to independently develop a model proposing that nucleons themselves are made up of constituent components, called quarks, bound together by the exchange of gluons [1]. This lead to the development of the fundamental theory of the strong interaction, known as Quantum Chromo-Dynamics (QCD). It is now a strong goal of the nuclear physics community to understand the interactions of quarks and gluons and how those interactions make manifest both nucleons themselves, which account for nearly all the mass of the visible matter in the universe, as well as the nucleons' spin, mass, magnetic moment, and nuclear binding energy. Because of the well-known properties of the electromagnetic interaction, electron scattering is an ideal process for such studies.

Although it would theoretically be possible to study these properties using fixed-target electron beam experiments, it is three-fold prohibitive: it is much more costly to construct an accelerator to accelerate electrons to the necessary momentum (on the order of TeV) than to build a collider, it is more difficult and complicated to do transverse nucleon polarization studies with a fixed target due to the nature of the required magnetic fields, and it is very difficult to study the target fragments of a fixed target reactions due to final state interactions whereas in a collider the fragments will be boosted in the same direction as the ion beam. It was therefore deemed a priority by the 2007 Nuclear Science Advisory Committee's Long-Range Plan that an Electron-Ion Collider (EIC) be the next facility to be built in the United States [2].

The EIC will not be the first facility to have the capability of colliding electrons and positrons with protons. The HERA accelerator in Hamburg, Germany was the world's first electron-proton collider, reaching electron energies of up to 28 GeV and protons to nearly 1 TeV with a luminosity on the order of $10^{31} \text{ cm}^{-2} \text{ s}^{-1}$ before shutting down in 2007. Figure 2.1 shows the combined H1 and Zeus experimental data from HERA for the measurement of the structure function for positron-proton scattering along with fixed target data for a wide range of both x and Q^2 . The EIC hopes to improve upon the already rich science produced at HERA threefold: by increasing the luminosity of the accelerator to on the

order of $10^{34} \text{ cm}^{-2} \text{ s}^{-1}$, by allowing for the use of heavier ion beams such as oxygen, and by allowing for both transversely and longitudinally polarized beams of electrons and light ions. With these improvements the EIC will be able to look into hadronic final states with much greater detail.

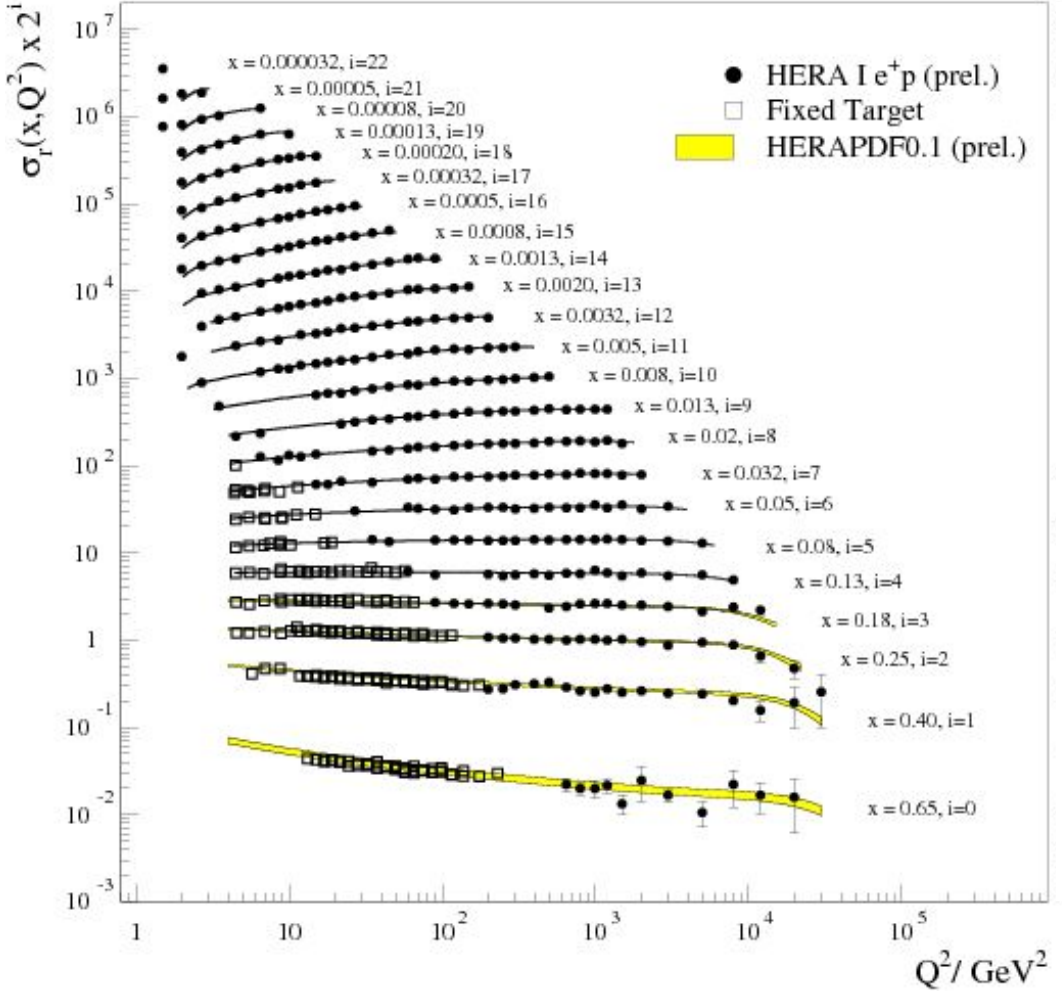


FIG. 2.1: The reduced cross section $\sigma_r(x, Q^2)$ as a function of Q^2 . Filled circles are combined H1 and Zeus data from HERA for proton-positron collisions, hollow squares are from fixed target experiments, and the yellow is prediction from HERAPDF0.1

2.1 SCIENCE GOALS

The goal of an EIC will be to find out how QCD is responsible for the structure and dynamics of nucleons, the nature of the nucleon-nucleon force, and the relative importance of the valance quarks.

2.1.1 NUCLEON SPIN

One major question still pestering nuclear physicists is “What is the origin of the nucleon spin?”. In the 1980s the naive answer was that the total nucleon spin was the sum of the spin of its three valence quarks, but many years of experimentation has revealed that it is much more complicated (Fig. 2.2), with the contributions from gluons and orbital angular momentum still in question. The EIC will be capable of much more detailed study of the contributions to the nucleon structure by enabling multi-dimensional projections of the distribution of quarks and gluons in space, longitudinal and transverse momenta, spin, and flavor.

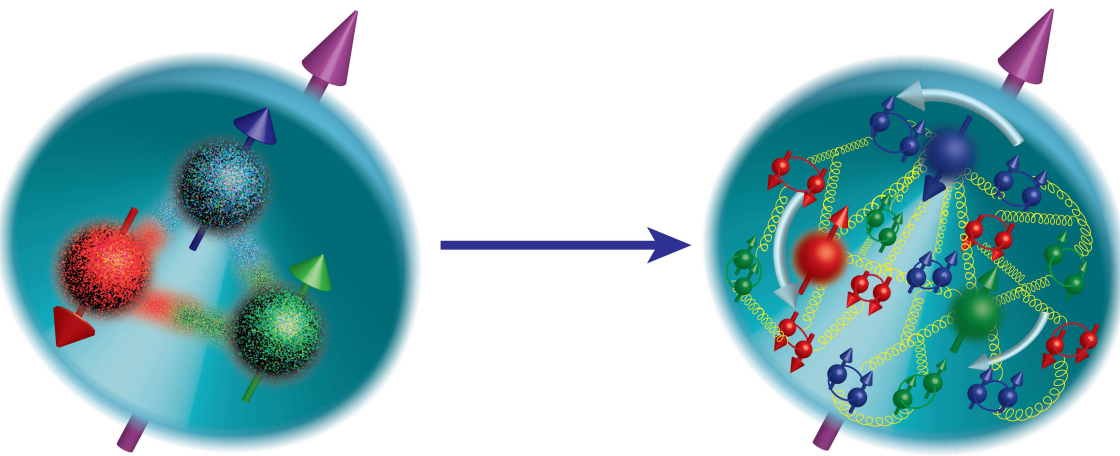


FIG. 2.2: Evolution of our understanding of nucleon spin structure. **Left:** In the 1980s, a nucleon's spin was naively explained by the alignment of the spins of its constituent quarks. **Right:** In the current picture, valence quarks, sea quarks and gluons, and their possible orbital motion are expected to contribute to overall nucleon spin.

2.1.2 THE EMC EFFECT

It was first observed by the European Muon Collaboration (EMC), and confirmed by other experiments that there is a modification between the nucleon structure function, F_2 , of deuterium to those of heavier elements as a function of Bjorken x [3]. Figure 2.3 shows the ratio of structure functions of Carbon and Deuterium for $0.2 < x < 0.9$. Initial assumptions were that this ratio of structure functions would be unity, but measurements have clearly shown a suppression in this ratio for $0.3 < x < 0.8$.

The reason for this modification to the nuclear structure function is still a mystery, but the

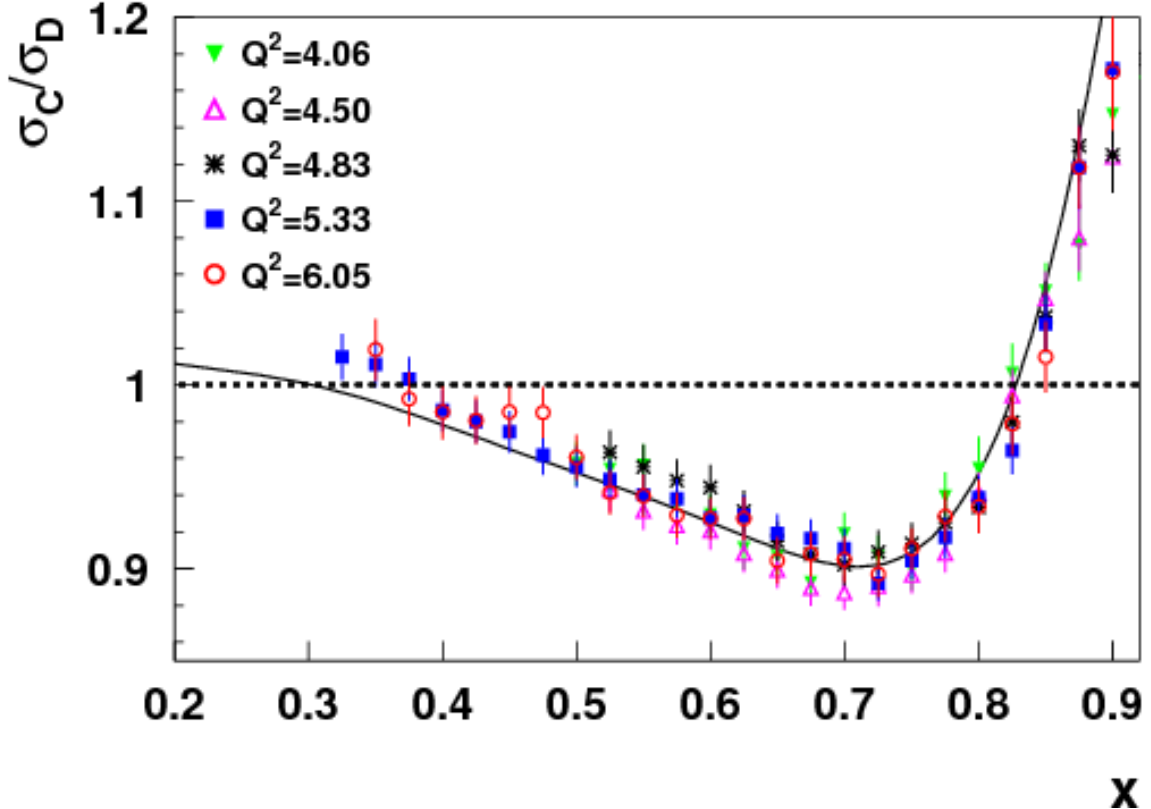


FIG. 2.3: Ratio of the nucleon structure functions for carbon and deuterium for $0.2 < x < 0.9$ and a range of Q^2 values.

EIC hopes to shed light on this phenomenon by studying various coherent exclusive reactions, such as J/Ψ production, which could allow for the quantification of initial conditions in heavy-ion collisions by mapping out the geometry of the nucleus in high-energy processes. This mapping can also help to understand other collective dynamics, such as shadowing and anti-shadowing.

2.1.3 GLUON DISTRIBUTIONS INSIDE NUCLEI

As mentioned above, the EMC effect, the modification of the distribution of quarks in a nucleus versus their distribution in nucleons, is a known (yet still mysterious) phenomenon. It is suspected that this modification also occurs for gluons, with experiments such as ALICE showing evidence for gluon shadowing for $x \approx 10^{-3}$ [4]. The EIC hopes to measure this suppression of the structure functions thanks to its wider range of kinematics both in x and Q^2 , allowing not only for the measurement of gluon shadowing ($x < 0.05$), but also

anti-shadowing ($x \approx 0.1$), and possibly the EMC effect for gluons ($x > 0.3$), shedding light on the origins of the EMC effect.

2.2 FACILITIES

As of the writing of this thesis there are two competing designs for an EIC facility to be built in the United States: a figure-8 accelerator design for Thomas Jefferson National Accelerator Facility (JLab) (Figure 2.5), and a ring-ring accelerator design for Brookhaven National Lab (BNL) (Figure 2.6).

The JLab EIC (JLEIC) is planned to be approximately 1.4 km in circumference and have a footprint of roughly 500 m by 170 m. The design is a ring-ring with electrons and ions being stored in separate beam lines and collided at two interaction points (IPs) (outlined in red in Figure 2.5) on the figure-8. The JLab CEBAF SRF linac will be used as an electron injector for electrons with 3 - 11 GeV energy. The second ring will store an ion beam with energy of 20 to 100 GeV for protons or up to 40 GeV per nucleon for light to heavy ions. The ion beams are generated and accelerated in a new ion injector complex with the same figure-8 design that will be utilized to preserve ion polarization. The two rings will be stacked vertically in the same underground tunnel [5].

The BNL facility, named eRHIC, will use a new electron beam facility based on an Energy Recovery LINAC that will be built inside of the Relativistic Heavy Ion Collider (RHIC) tunnel to collide with RHIC's pre-existing polarized proton/ion beam. The existing hadron ring will accelerate protons up to 250 GeV/c, ${}^3\text{He}^{+2}$ up to 167 GeV/c per nucleon, and heavier ions (e.g. gold or uranium) up to 100 GeV/c per nucleon. The new electron ring will be capable of producing electrons from 2 - 21 GeV/c [6]. Figure 2.6 shows the current design layout of the eRHIC facility (top) and the Brookhaven eA Solenoidal Tracker (BeAST) detector proposed for the interaction region (bottom).

2.2.1 PARTICLE IDENTIFICATION REQUIREMENTS AND SOLUTIONS

The large center of mass energies and diverse physics program at an EIC necessitate a very sophisticated detector suite. The most basic process that the EIC will observe is inclusive Deep Inelastic Scattering (DIS). This process will produce many different combinations of final-state hadrons over a wide angular distribution for a given kinematic setting of x and Q^2 . Coupled with the large beam energies, there is a need of PID over a large range in the hadron endcap (up to 50 GeV/c), range up to the beam energy in the electron endcap (up to 12 GeV/c), and a moderate range in the central barrel region (up to 6 GeV/c). The ability

to accurately identify hadrons in the final state is therefore a key requirement for the physics program, as is shown by Figure 2.4 which shows the momentum distributions of pions and kaons for each region of interest for typical beam energies for both BNL and JLab.

As can be seen in Figures 2.5 and 2.6, the layouts of the two detector concepts for JLab and BNL are slightly different, but the solutions for PID requirements are very similar. In the hadron endcap, because of the large final state energies the ideal PID detector would be a gaseous, mirror-based Ring Imaging Cherenkov (RICH) detector which would be capable of the required 50 GeV/c momentum resolution. The hadrons produced going towards the electron endcap scales in both energy and quantity with the energy of the electron beam energy. Although the maximum electron beam energies of JLab and BNL differ, a 10 GeV/c momentum resolution seems to be suitable for both facilities, and so a modular aerogel RICH detector is currently under development. In the central barrel region the necessary momentum coverage is not as high as that of the endcaps because the transverse momentum transfer from the electron beam to the ion beam is relatively small, on the order of 7 GeV/c. This smaller momentum range coupled with a smaller space to fit a detector make a detector based on Detection of Internally Reflected Cherenkov light (DIRC) technology, the main subject of this thesis, an ideal solution for PID in this region.

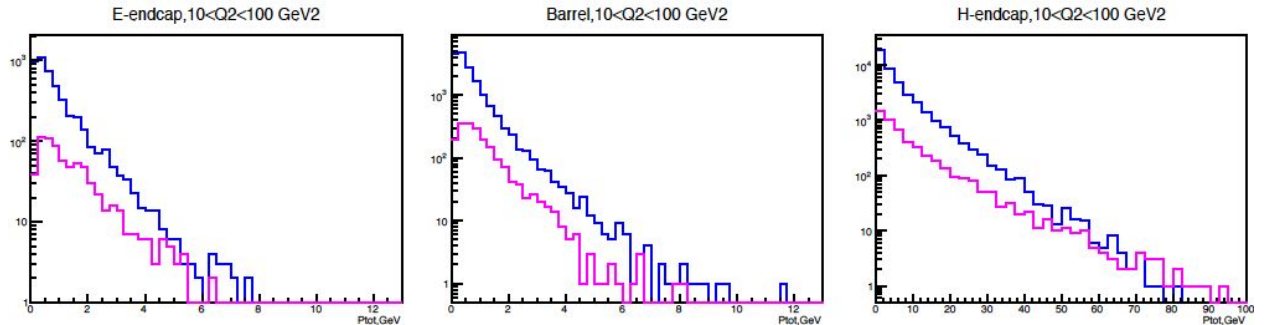


FIG. 2.4: Momentum distributions for pions (blue) and kaons (magenta) from the pythia simulation package for DIS events corresponding to collisions between 10 GeV electrons and 100 GeV protons, a common BNL/JLab kinematic, shown for a bin of $10 < Q^2 < 100 \text{ GeV}^2$.

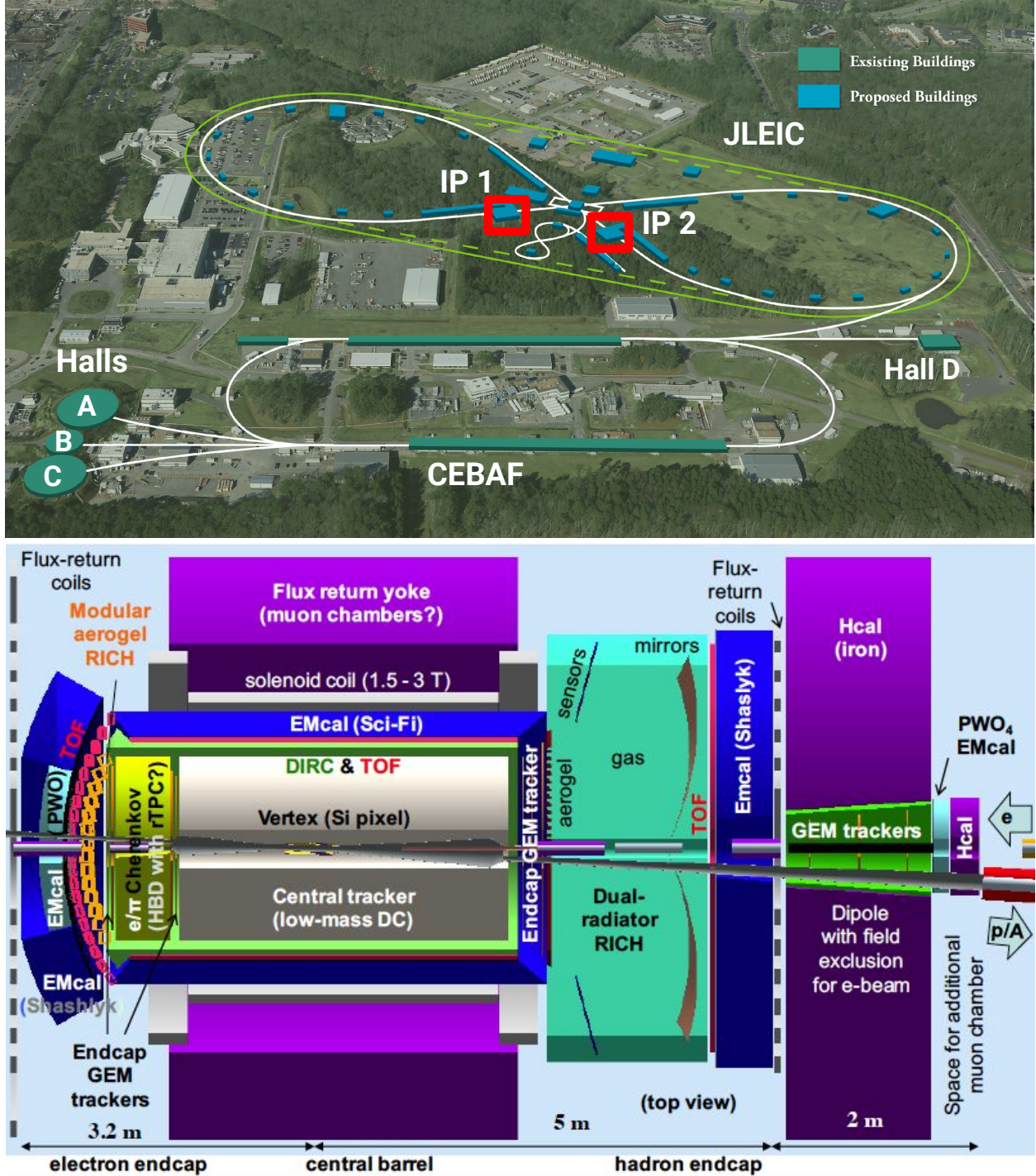


FIG. 2.5: Current design of the EIC facility for JLab with the two interaction points (IPs) highlighted in red (top), and the current baseline design for the detector at IP1 (bottom).

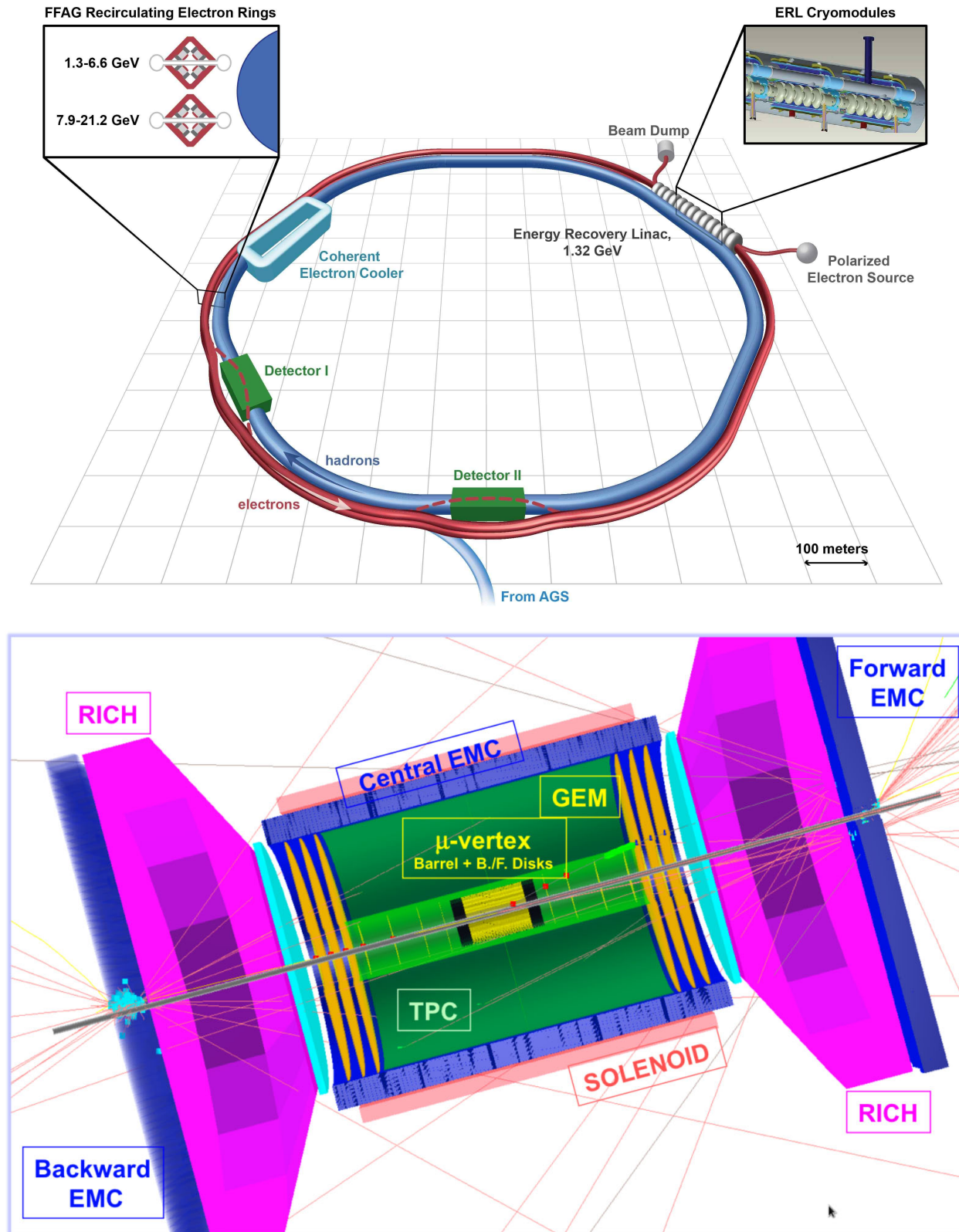


FIG. 2.6: Current design of the EIC facility at BNL (top), and the proposed BeAST (Brookhaven eA Solenoidal Tracker) detector (bottom).

CHAPTER 3

DIRC TECHNOLOGY

DIRC detectors are based on the concept of the Detection of Internally Reflected Cherenkov light (DIRC) produced in a solid radiator bar to identify charged particle. It is a special type of Cherenkov counter, which uses the unique properties of Cherenkov radiation to identify charged particle species.

3.1 CHERENKOV RADIATION

Einstein postulated in his Theory of Relativity that the speed of light in a vacuum, c , is the limit of the velocity of massive particles. In an optically transparent medium, however, the speed at which light propagates is modified: $c_{med} = c/n$, where n is the index of refraction of the medium. Pavel Cherenkov discovered in 1934 that massive particles moving through a medium faster than the speed of light in that medium emit light in the form of now-called Cherenkov radiation. Cherenkov was able to establish several interesting properties of this radiation: it is only emitted from charged particles above a certain velocity threshold $v > c/n$, the intensity is proportional to the particle's path length, emission is prompt, and the light is polarized with a continuous wavelength spectrum. Later in 1937 Ilya Frank and Igor Tamm theoretically formulated this radiation with fantastic agreement to Cherenkov's findings, and the three shared the 1958 Nobel Prize in Physics for their efforts [7].

Further studies confirmed that Cherenkov radiation is emitted uniformly in azimuth (ϕ_c) around the particle's direction of travel with the polar opening angle θ_C defined as

$$\cos \theta_C = \frac{1}{\beta n(\lambda)}, \quad (3.1)$$

where $\beta = v_p/c$, v_p is the particle's velocity, and the index of refraction is a function of the emitted photon wavelength. In a normal, dispersive optical medium the opening half-angle of the shock wave produced by the Cherenkov radiation, η_C defined in Figure 3.1, is not complementary to the Cherenkov angle. The relationship between the two is given by

$$\cot \eta_C = \left[\frac{d}{d\omega} (\omega \tan \theta_C) \right]_{\omega_0} = \left[\tan \theta_C + \beta^2 \omega n(\omega) \frac{dn}{d\omega} \cot \theta_C \right]_{\omega_0} \quad (3.2)$$

where ω_0 is the central value of the considered frequency range. Because the second term in (3.2) is zero only for non-dispersive media the shock wave front is not perpendicular to the Cherenkov cone in real detectors.

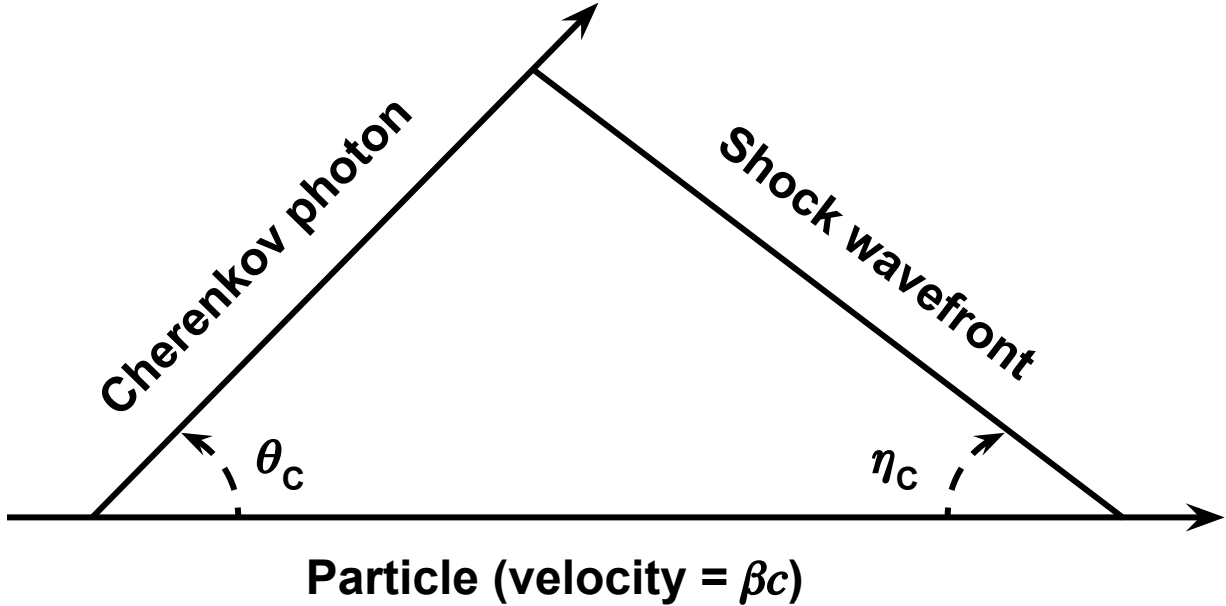


FIG. 3.1: Illustration of the Cherenkov cone.

Because particles lose very little energy when radiating Cherenkov photons the emission is very weak. The number of photons $N_{photons}$ emitted per path length L (in cm) by a moving particle with charge z is given by the Frank-Tamm equation

$$\frac{N_{photons}}{L} = \frac{\alpha^2 z^2}{r_e m_e c^2} \int \sin^2 \theta_C(E) dE \quad (3.3)$$

where E is the photon energy in eV, the integral is taken over the region where $n(E)$ is greater than 1, and $\frac{\alpha^2 z^2}{r_e m_e c^2} = 370 \text{ cm}^{-1} \text{ eV}^{-1}$.

3.2 APPLYING THE CHERENKOV EFFECT TO PARTICLE ID

In order to identify particle species one must know both the mass and charge of the particle in question. Because the Cherenkov angle encodes the particle's velocity it is, in principle, a simple matter to measure the particle's momentum with a tracking chamber as well as the velocity obtained from (3.1) to determine the mass and charge. Figure 3.2 shows how different particle species can be distinguished for a given momentum in fused silica.

Threshold Cherenkov counters are detectors used for particle identification (PID) by exploiting the fact that only particles above the threshold velocity $\beta > 1/n$ will emit Cherenkov photons. The information about a particle's velocity can be combined with momentum information from a tracking system to determine the mass as [8]

$$m = \frac{p}{c} \sqrt{n^2 \cos^2 \theta_C - 1} \quad (3.4)$$

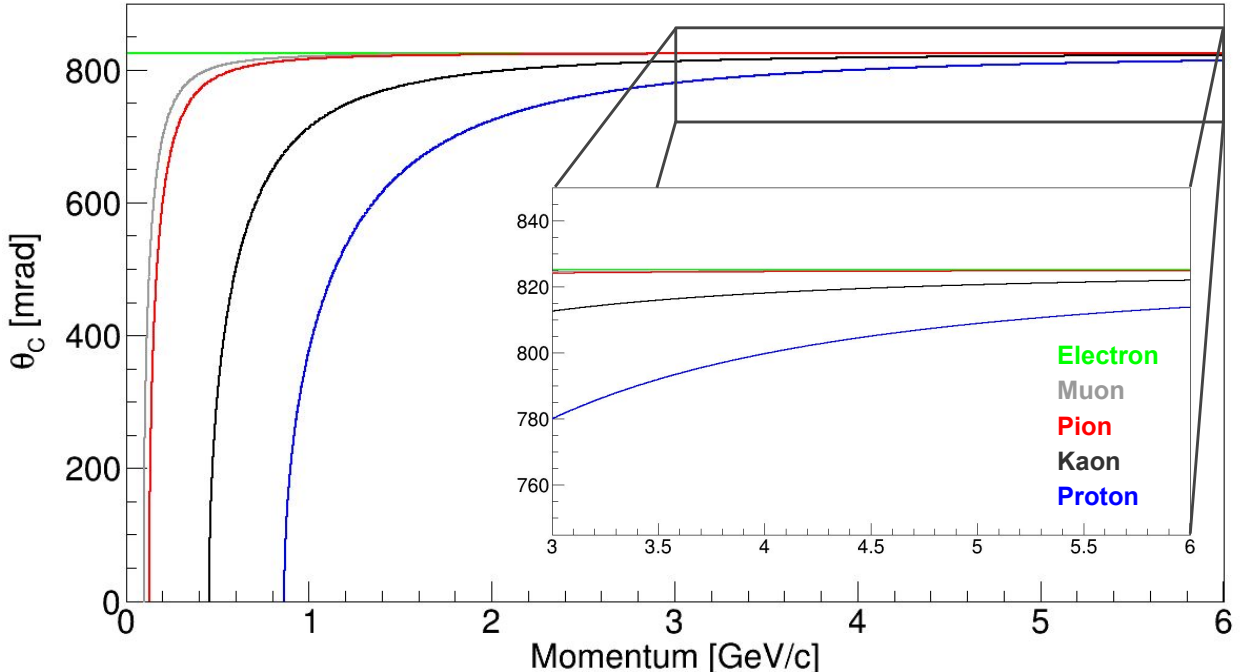


FIG. 3.2: Particle momentum [GeV/c] versus Cherenkov angle [mrad] for different particle species in fused silica ($n \approx 1.473$). The zoomed image shows that it is indeed possible to differentiate pions, kaons, and protons at higher particle momenta.

3.3 RING IMAGING DETECTORS

Ring Imaging Cherenkov (RICH) detectors are designed to efficiently identify and separate different particle species over a wide range of momenta. A basic RICH system is shown in Figure 3.3.

A volume of radiator, either gaseous (e.g. C_4F_{10}) or solid (e.g. aerogel), is positioned upstream of an array of photosensors. A charged particle traveling through a thin radiator above the threshold velocity will continuously emit Cherenkov photons in a cone. The resulting image on the photosensor array is an annulus of thickness $d \tan \theta_C$ and an inner

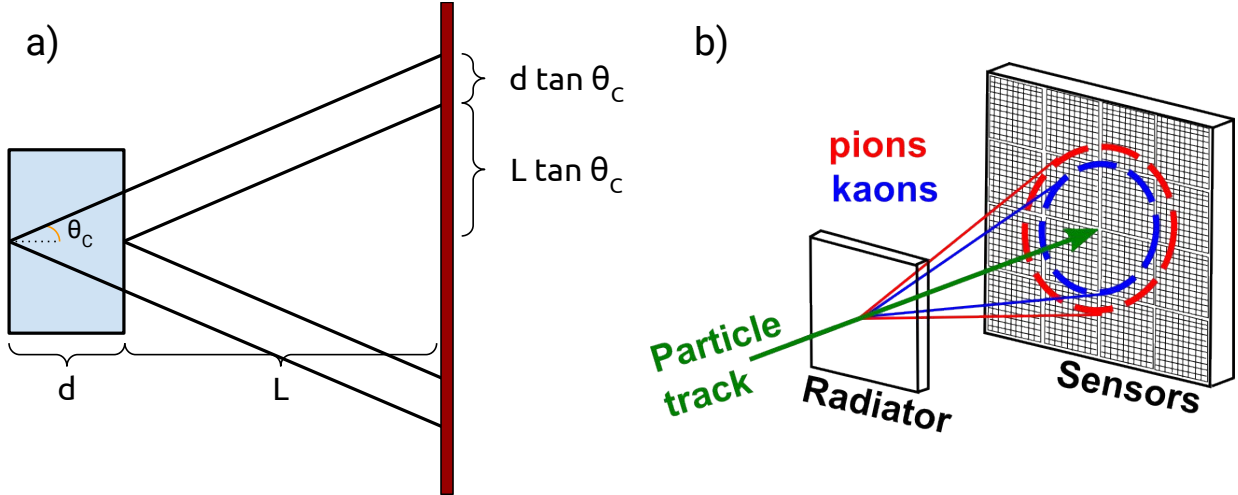


FIG. 3.3: Basic concept of a proximity focusing Ring Imaging Cherenkov (RICH) detector (a), and an example of how they can be used to do PID based on particle mass (b).

radius of $L \tan \theta_C$, where d is the distance the particle traveled inside the radiator, L is the distance between the radiator and the photosensors, and θ_C is the usual Cherenkov angle (Figure 3.3b). PID is done by measuring the average radius of the annulus and reconstructing the Cherenkov angle geometrically.

3.4 DIRC DETECTORS

DIRC detectors work much the same way as a RICH in that collect Cherenkov photons produced from a radiating material and use the created image on the photosensors to reconstruct the Cherenkov angle. In the case of a DIRC, the radiating medium is also used as a light guide as some of the Cherenkov photons undergo total internal reflection inside the radiator and are guided towards one end of the radiator to a readout (Figure 3.4). The radiator of choice is a solid bar made of fused silica, with an index of refraction $n \approx 1.473$. A rectangular cross section and highly smoothed and polished sides ensure that the magnitude of the Cherenkov angle is preserved during internal reflection. Photons that are created propagating away from the readout are reflected back towards the readout by a mirror. Once the photons exit the radiator they are allowed to separate through an expansion volume before being imaged in both (x, y) position as well as time. The arrival position and propagation time of each detected photon are combined with tracking information to reconstruct the Cherenkov angle and determine the corresponding PID likelihoods (reconstruction methods and techniques for DIRC detectors will be discussed in detail in Chapter 6).

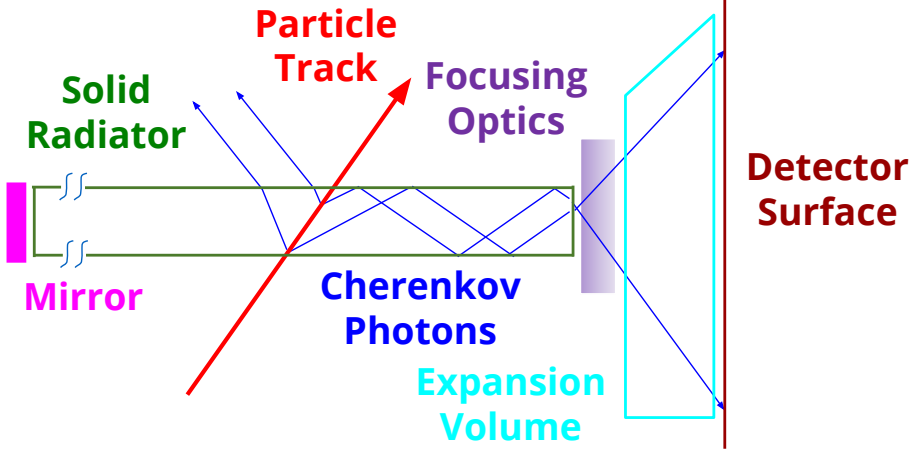


FIG. 3.4: The basic components of a DIRC detector: a solid radiator, typically fused silica (green); a mirror to redirect backward-going photons (pink); optional focusing optics (purple); an expansion volume to allow photons to separate in space (cyan); and a detector surface to record the position and arrival time of Cherenkov photons (maroon).

The performance of a DIRC detector is given by the resolution in the Cherenkov polar opening angle of the particle track, $\sigma_{\theta_C, \text{track}}^2$, which can be written as:

$$\sigma_{\theta_C, \text{track}}^2 = \sigma_{\theta_C}^2 / N_\gamma + \sigma_{\text{correlated}}^2 \quad (3.5)$$

where σ_{θ_C} is the average single photon Cherenkov angle resolution, N_γ is the number of measured photons per track, and $\sigma_{\text{correlated}}$ includes several correlated terms that contribute to the resolution such as the uncertainty in the particle track direction coming from external tracking systems. Because the track direction is crucial to the reconstruction of the Cherenkov angle, this error needs to be small for the performance to not suffer. For the EIC a tracking resolution on the order of 1 mrad is required for adequate PID.

As of the writing of this thesis the only DIRC detector used in a full experiment is the BaBar DIRC at SLAC National Accelerator Laboratory, which was successfully operated from 1999 through 2008 [9]. It proved to be a robust, stable, and easy to operate system for more than 8 years, providing excellent pion/kaon separation for all tracks from B -meson decays. It used 4.9 m long radiator bars with a rectangular cross section of $17.25 \times 35 \text{ mm}^2$. Each bar was made of four 1.225 m long fused silica bars glued end-to-end. The bars were placed in 12 hermetically sealed containers, called bar boxes, each holding 12 radiator bars for a total of 144 bars. At the end of each box was attached a wedge of fused silica and a window to allow the photons to expand before entering the water-filled expansion volume and being

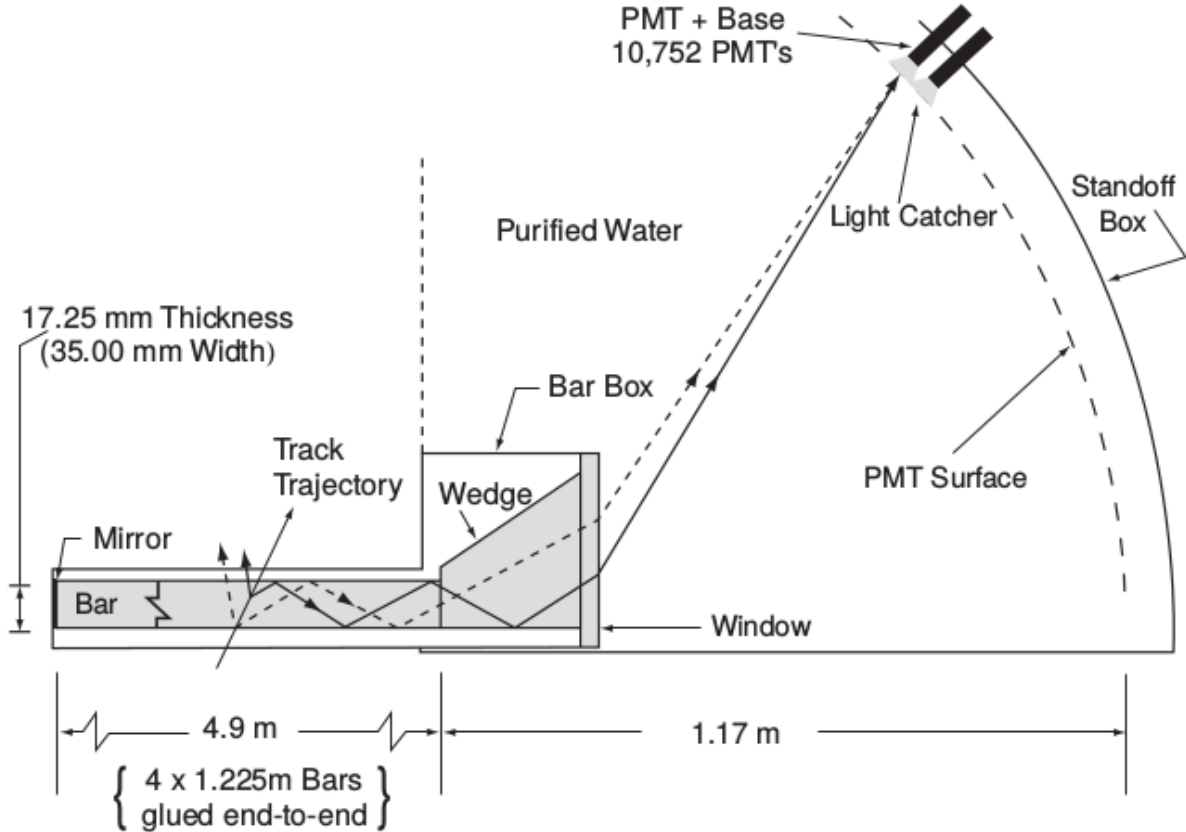


FIG. 3.5: Schematic of BaBar DIRC and imaging region.

read out on one of 10,752 photomultiplier tubes (see Figure 3.5). Figure 3.6 summarizes the performance of the BaBar DIRC, showing excellent Cherenkov angle reconstruction (2.5 mrad, only 14% larger than the design goal of 2.2 mrad) and photon yield per track.

3.4.1 DIRCS IN FUTURE EXPERIMENTS

The BaBar DIRC has since inspired many other experiments/facilities, including the EIC, to utilize this new, novel PID system in a variety of ways (Figure 3.7). The Focusing DIRC (FDIRC) proposed for the now-cancelled SuperB collider in Italy was the first to propose using some form of focusing for the Cherenkov photons, allowing for a factor of 10 smaller expansion volume [10]. The barrel DIRC for the PANDA experiment at FAIR in Germany will use shorter radiator bars for a more compact design [11], while the PANDA disc DIRC will be used in the forward region and will be the first disc DIRC to be used

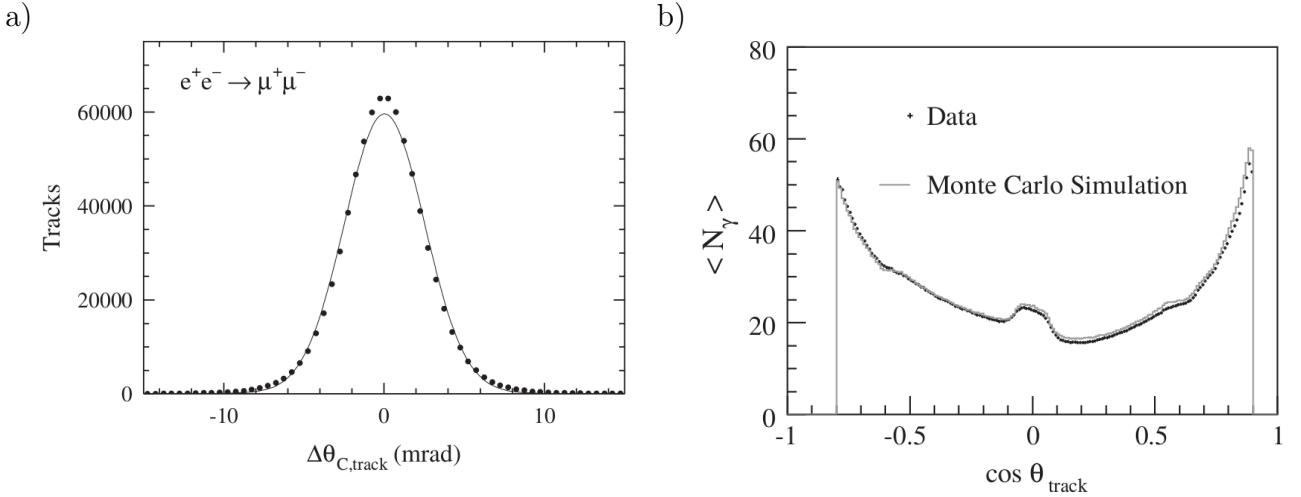


FIG. 3.6: Performance of the BaBar DIRC for $e^+e^- \rightarrow \mu^+\mu^-$ events. a) shows the difference between the measured and expected Cherenkov angle (dots) and a Gaussian fit to the data with a 2.5 mrad width (line). b) is the average number of detected photons vs. track polar angle for data (dots) and Geant4 simulation (line).

in a high-performance 4π detector [12]. Belle II at the SuperKEKB accelerator in Japan will utilize wide plates as radiators and focus on fast timing for PID in the barrel region [13]. The TORCH detector, similar to the PANDA disc DIRC, will be a large-area detector focusing on precision time-of-flight to do PID for low momentum kaons at the upgraded LHCb experiment [14]. The GlueX experiment at JLab will be recycling four bar boxes from the BaBar experiment to cover the forward region of their spectrometer; utilizing focusing similar to the FDIRC design [15].

3.5 HIT PATTERNS AND CHERENKOV ANGLE RECONSTRUCTION METHODS

As mentioned previously, a DIRC detector is a more compact RICH system that relies on internal reflection of the Cherenkov photons inside the radiating material. However, as is illustrated in Figure 3.4, not all of the light produced inside the radiator is internally reflected as photons with an angle less than the critical angle (approximately 43 degrees for the interface from fused silica to air) with respect to the surface will escape the radiator. Because of this loss of photons the hit pattern of a DIRC is only roughly half of a typical RICH ring. To complicate matters further, the image of this half ring is doubled depending on if the photon exiting the bar was last reflected from the top or bottom of the radiator

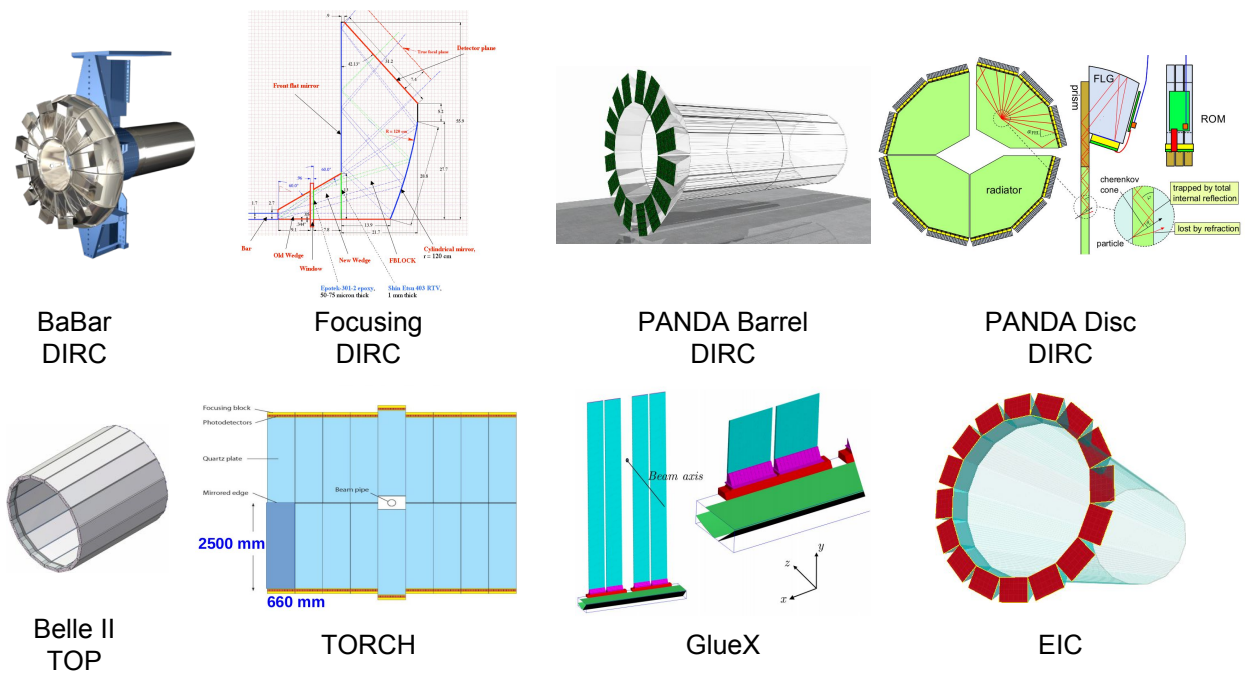


FIG. 3.7: Evolution of the DIRC concept. From top left to bottom right: BaBar Barrel DIRC, Focusing DIRC, PANDA Barrel DIRC, PANDA Disc DIRC, Belle II Time of Propagation DIRC, LHCb TORCH DIRC, GlueX DIRC, EIC DIRC

CHAPTER 4

HIGH-PERFORMANCE DIRC@EIC

4.1 EVOLUTION OF THE DIRC@EIC DESIGN

4.2 CURRENT HIGH-PERFORMANCE DIRC DESIGN

4.3 SIMULATED PERFORMANCE

4.4 POTENTIAL OPTIMIZATIONS

CHAPTER 5

TESTING DIRC COMPONENTS

The validation of key components of the DIRC for an EIC is vital to show that the Geant4 simulation package produces results expected for the real detector. However, due to budget restraints it was not possible to build or otherwise procure a full scale prototype of the envisioned EIC DIRC discussed in Chapter 4 (e.g. 2 mm pixel MCP-PMTs are not available on the market). Instead a series of test bench measurements were made for both the NLaK33 material of the 3-layer lens and for the performance of similar MCP-PMTs in high magnetic field environments.

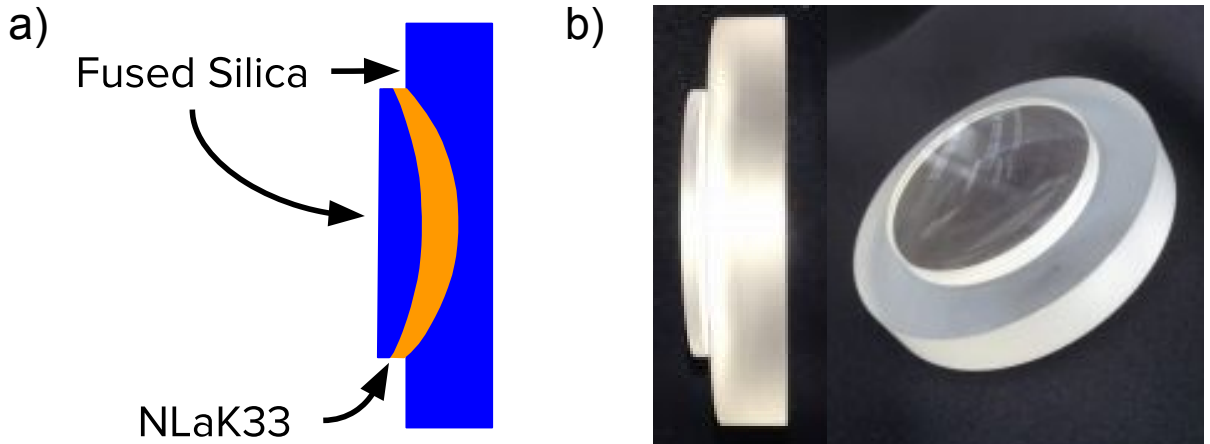


FIG. 5.1: Schematic drawing of the 3-layer lens design with two layers of fused silica sandwiching a layer of high refractive index NLaK33 glass (a), and a side and front view of a prototype lens built for testing (b).

5.1 OPTICAL PROPERTIES OF 3-LAYER LENS

The FDIRC R&D program first developed the concept of using focusing mirrors for DIRC detectors. The PANDA Barrel DIRC group settled on using a focusing lens between the radiator bar and the expansion volume. A standard lens made of fused silica with an air gap between the lens and the expansion volume was first studied. Figure 5.2 shows that while this air gap lens provides good focusing of the Cherenkov pattern in the central region of the ring, it becomes defocused nearer to the edges of the pattern and loses photons due to

either internal reflections in the lens due to the jump in index of refraction, or from photons at steeper angles exiting the lens and missing the expansion volume entirely.

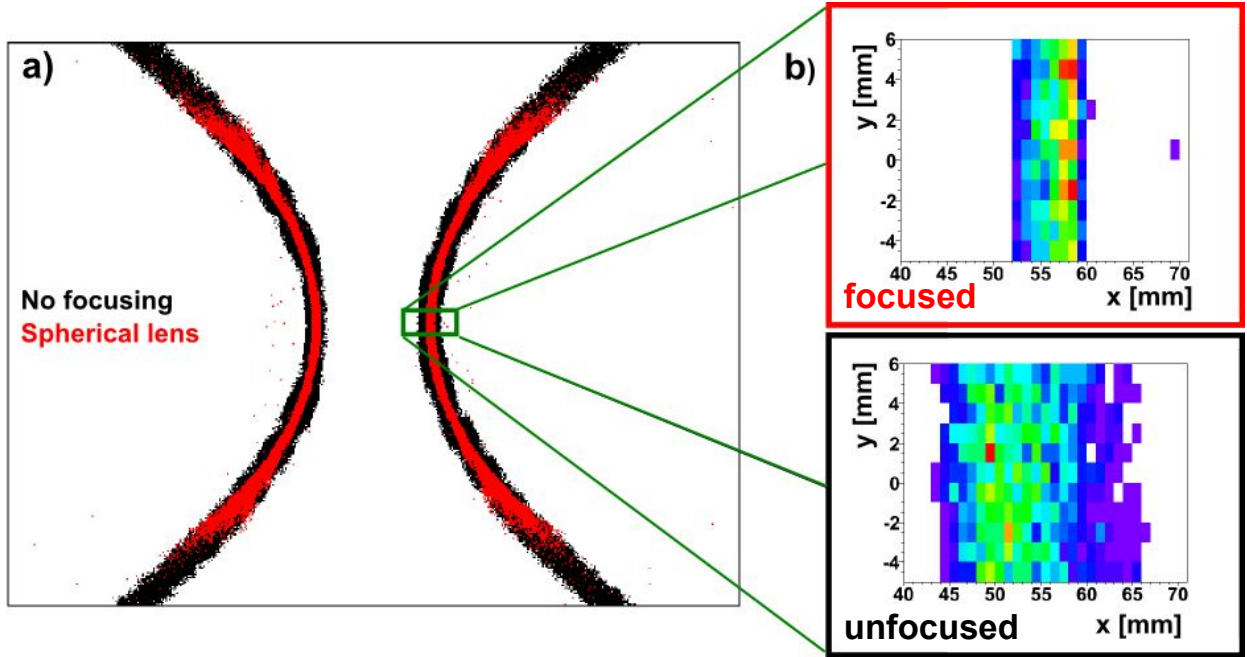


FIG. 5.2: Simulated hit pattern of PANDA DIRC without (black) and with (red) air gap lens focusing (a). On the outer edges of the ring image the lens is becoming dispersive and losing photons, while near the center of the rings the lens does a good job of focusing the image, as seen more clearly in b).

Next a 2-layer lens

The advantage of this 3-layer lens design over a traditional optical lens or a 2-layer lens is the shape of the focal plane. According to simulation the focal plane of the 3-layer lens is relatively flat, as shown in Figure 5.3.

5.2 RADIATION HARDNESS OF NLAK33 MATERIAL

5.3 PERFORMANCE OF MCP-PMTS IN HIGH MAGNETIC FIELD

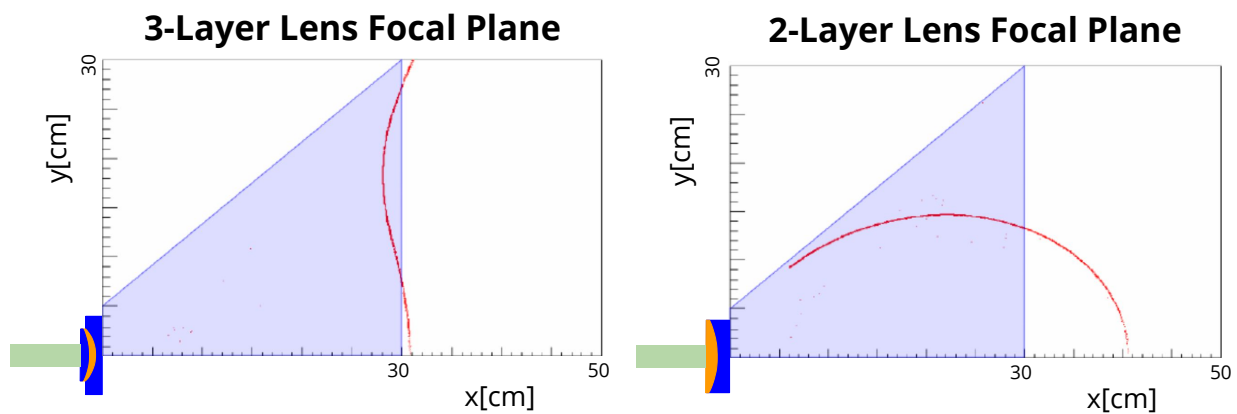


FIG. 5.3: The simulated focal planes (red lines) of the 3-layer lens (left) and a 2-layer lens (right) compared to the shape of the expansion volume prism (grey). Obviously the focal plane of the 2-layer lens is highly parabolic in shape, whereas the 3-layer lens focal plane is relatively flat, allowing for a better resolution of the Cherenkov angle.

CHAPTER 6

3-LAYER LENS PERFORMANCE IN PARTICLE BEAM

6.1 PROTOTYPE SETUP

6.2 SIMULATED PERFORMANCE

6.3 DATA ANALYSIS

6.3.1 ERROR EVALUATION

CHAPTER 7

OUTLOOK AND SUMMARY

BIBLIOGRAPHY

- [1] Bill Carithers and Paul Grannis. Discovery of the top quark. *Beam Line*, 25(3):4–16, 1995.
- [2] Robert Tribble et. al. *Frontiers of Nuclear Science*. 2007.
- [3] L. B. Weinstein, E. Piasetzky, D. W. Higinbotham, J. Gomez, O. Hen, and R. Shneor. Short Range Correlations and the EMC Effect. *Phys. Rev. Lett.*, 106:052301, 2011.
- [4] V. Guzey, E. Kryshen, M. Strikman, and M. Zhalov. Evidence for nuclear gluon shadowing from the ALICE measurements of PbPb ultraperipheral exclusive J/ψ production. *Phys. Lett.*, B726:290–295, 2013.
- [5] S. Abeyratne et al. MEIC Design Summary. 2015.
- [6] E. C. Aschenauer et al. eRHIC Design Study: An Electron-Ion Collider at BNL. 2014.
- [7] Alan A. Watson. The Discovery of Cherenkov Radiation and its use in the detection of extensive air showers. *Nucl. Phys. Proc. Suppl.*, 212-213:13–19, 2011.
- [8] Claus Grupen and Irene Buvat, editors. *Handbook of particle detection and imaging*, vol. 1 and vol.2. Springer, Berlin, Germany, 2012.
- [9] Jochen Schwiening. Construction and Performance of the BaBar DIRC. *JINST*, 4:P10004, 2009.
- [10] *The Focusing DIRC - the First RICH Detector to Correct the Chromatic Error by Timing, and the Development of a New TOF Detector Concept*, 2007. [Submitted to: Nucl. Instrum. Meth.(2007)].
- [11] R. Dzhygadlo et al. The PANDA Barrel DIRC. *JINST*, 11(05):C05013, 2016.
- [12] *Proceedings, Workshop on Fast Cherenkov Detectors: Photon detection, DIRC design and DAQ (DIRC2015)*, volume 11, 2016.
- [13] E. Torassa. Particle identification with the TOP and ARICH detectors at Belle II. *Nucl. Instrum. Meth.*, A824:152–155, 2016.

- [14] K. Fhl et al. TORCH - Cherenkov and Time-of-Flight PID Detector for the LHCb Upgrade at CERN. *JINST*, 11(05):C05020, 2016.
- [15] J. Stevens et al. The GlueX DIRC Project. *JINST*, 11(07):C07010, 2016.

APPENDIX A

ERROR EVALUATION

VITA

S. Lee Allison
Department of Physics
Old Dominion University
Norfolk, VA 23529

The text of the Vita goes here.